ACS OMEGA

http://pubs.acs.org/journal/acsodf

Article

New Method for the Synthesis of 2D Vanadium Nitride (MXene) and Its Application as a Supercapacitor Electrode

Sandhya Venkateshalu, Jayesh Cherusseri, Manickavasakam Karnan, Kowsik Sambath Kumar, Pratap Kollu, Marappan Sathish, Jayan Thomas, Soon Kwan Jeong,* and Andrews Nirmala Grace*

Cite This: *ACS Omega* 2020, 5, 17983−17992

Read Online

ACCESS | Metrics & More | Article Recommendations | Supporting Information

ABSTRACT: MXenes are the class of two-dimensional transition metal carbides and nitrides that exhibit unique properties and are used in a multitude of applications such as biosensors, water purification, electromagnetic interference shielding, electrocatalysis, supercapacitors, and so forth. Carbide-based MXenes are being widely explored, whereas investigations on nitride-based ones are seldom. Among the nitride-based MXenes obtained from their MAX phases, only Ti_4N_3 and Ti_2N are reported so far. Herein, we report a novel synthesis of V_2NT_x (T_x is the surface termination) obtained by the selective removal of "Al" from V_2AlN by immersing powders of V_2AlN in the LiF−HCl mixture (salt−acid etching) followed by sonication to obtain V_2NT_x (T_x = −F, −O) MXene which is then delaminated using the dimethyl sulfoxide solvent. The V_2NT_x MXene is characterized by X-ray diffraction studies, field emission scanning electron microscope imaging, energy-dispersive X-ray spectroscopy, X-ray photoelectron spectroscopy, and high-resolution transmission electron microscope imaging. Supercapacitor electrodes are prepared using V_2NT_x MXenes and their electrochemical performances are examined by cyclic voltammetry, galvanostatic charge/discharge measurement, and electrochemical impedance spectroscopy. The V_2NT_x MXene electrode exhibits a specific capacitance of 112.8 F/g at a current density of 1.85 mA/cm^2 with an energy and power density of 15.66 W h/kg and 3748.4 W/kg, respectively, in 3.5 M KOH aqueous electrolyte. The electrode exhibits an excellent capacitance retention of 96% even after 10,000 charge/discharge cycles. An asymmetric supercapacitor fabricated with V_2NT_x as a negative electrode and Mn_3O_4 nanowalls as a positive electrode helps obtain a cell voltage of 1.8 V in aqueous KOH electrolyte.

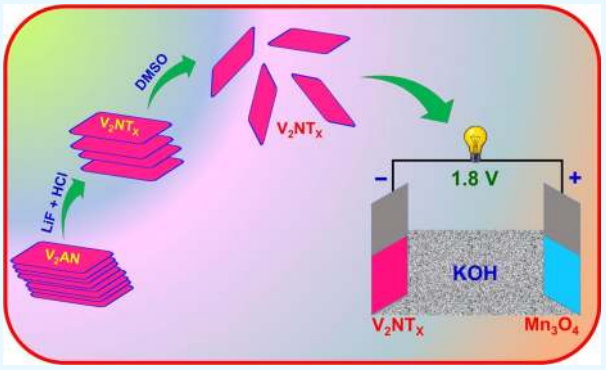

1. INTRODUCTION

Because of the imminent global energy crisis, research is being focused on developing efficient energy conversion and storage systems. Supercapacitors have been gaining much importance because of their high power densities and long cycle life.[1,2] Supercapacitors bridge the existing gap between batteries and capacitors, which exhibit characteristics of high energy density and high power density, respectively.[3] The performance of these supercapacitors can be enhanced by constructing them with efficient electrode materials.[4] In the recent years, two-dimensional (2D) materials have been gaining limelight with the excellent properties exhibited by graphene. Extensive studies have been carried out on 2D materials such as transition metal dichalcogenides (TMDs), hexagonal boron nitride, metal−organic frameworks, and the newly discovered MXenes as electrodes for supercapacitors. MXenes, discovered by the Gogotsi and Barsoum group in 2011, belong to the family of 2D materials, which includes transition metal nitrides, carbides, and carbonitrides.[5] MXenes are prepared by selective etching of A elements from 3D MAX phases, which has a general formula $M_{n+1}AX_n$ (n = 1, 2, and 3), where M, A, and X represent the *d*-block transition metals, group 13 or 14 elements, and either or both C and N atoms, respectively.[6] The new material MXene was named because of the loss of the A element from the parent MAX phase and its structure analogous to graphene. MAX phases are layered hexagonal structures with $P6_3/mmc$ symmetry, wherein the X atoms are sandwiched between the M layers and A atoms are present in the interleaved spaces of $M_{n+1}X_n$ layers.[7] The bond between M−X exhibits strong mixed covalent/ionic/metallic nature, whereas the bond between M−A is metallic in nature. Thus, the bonds in the MAX phases are highly strong to be broken but using the phenomenon of relative bond energies between M−A and M−X bonds, the "A" atoms can be selectively etched from the MAX phases by various chemical means without

Received: March 18, 2020
Accepted: July 2, 2020
Published: July 13, 2020

Scheme 1. Process Flow Indicating the Formation of V_2NT_x MXene

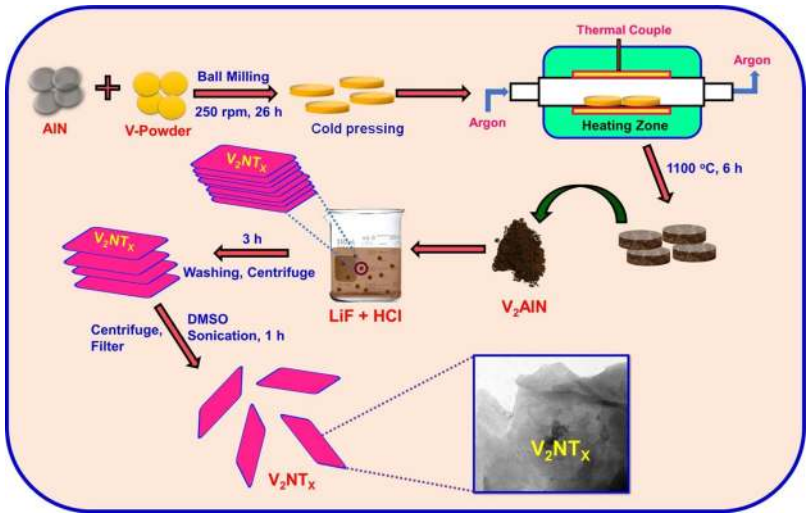

disrupting the M−X bonds.[8] After the etching process, chemically stable and closely packed MXenes with formula $M_{n+1}X_nT_x$ will be obtained, where T_x refers to the functional groups (−OH, −O, and −F) attached to the surface of the metal atoms after the etching procedure.[9]

Etching of "A" element from the MAX phase is the crucial step in the synthesis of MXene. The M−A bonds are weaker when compared to that of M−X bonds and the "A" element in the MAX phase can be etched through various methods reported in the literature. HF is the widely used etchant for carbide MXenes and its concentration, exposure time, and temperature are all crucial parameters in the process of etching.[10] Milder etchants such as $NaHF_2$, KHF_2, or NH_4HF_2 and a mixture of acid (H_2SO_4/HCl) and fluoride salt (NaF, KF, and LiF) have also been reported as effective etchants.[11] In the case of nitride MXenes, HF is incapable of etching "A" from their MAX phases because of its lower cohesive energies, which enables it to dissolve in HF. Urbankowski et al.[12] reported the synthesis of Ti_4N_3 using a eutectic mixture of molten salts as etching agents. The NaF−HCl mixture was used in the etching process by Soundiraraju and George to obtain Ti_2N.[13] In the current work, the LiF−HCl mixture was used as an etchant to obtain V_2N from V_2AlN. To obtain few-layered MXenes from the multilayered MXenes, usually, tetrabutylammonium hydroxide (TBAOH) and dimethyl sulfoxide (DMSO) are used as the delaminating agents.[12,13]

According to Barsoum and Radovic, more than 60 MAX phases exist till date but only a few MXenes from those are reported so far.[14] Many more MXenes are expected to be produced from their parent MAX phases in the future, thus providing a lot of scope in this field of research. Carbide- and carbonitride-based MXenes such as Ti_2C,[15] V_2C,[16] Nb_2C,[17] Mo_2C,[18] Ti_3C_2,[11] Zr_3C_2,[19] Nb_4C_3,[20] Ta_4C_3,[15] $Hf_3C_2T_z$,[21] TiNbC,[15] Mo_2TiC_2,[22] $(Ti_{0.5}Nb_{0.5})_2C$,[15] $(V_{0.5}Cr_{0.5})_3C_2$,[15] Mo_2ScC_2,[23] Cr_2TiC_2,[22] $Mo_2Ti_2C_3$,[22] $(Nb_{0.8}Ti_{0.2})_4C_3$,[20] $(Nb_{0.8}Zr_{0.2})_4C_3$,[20] and Ti_3CN[24] are some of the reported MXenes. Nitride-based MXenes have been rarely explored and only a few of them have been reported recently, viz., Ti_4N_3[12,25] and Ti_2N.[13,26] Nitride MXenes obtained by the ammonization of carbide MXenes have also been reported.[27]

MXenes have started gaining a lot of attention since its discovery and have been explored in various fields.[28] Xie et al. reported the use of MXenes as a promising electrode material for rechargeable non-lithium-ion batteries.[29] 2D Zr_2CO_2 and Hf_2CO_2 were proved as an efficient catalyst for high-efficiency photocatalytic water splitting, thereby enabling the production of hydrogen fuel.[30] The antibacterial properties of $Ti_3C_2T_x$ were explored against *Escherichia coli* and *Bacillus subtilis*, where it exhibited a higher antibacterial efficiency compared to graphene oxide.[31] A Ti_3C_2 MXene-FET biosensor developed by the Xu and group was successful in monitoring the activity in hippocampal neurons with high sensitivity through a label-free detection of dopamine.[32] The effectiveness of Ti_3C_2 in the absorbing and shielding of electromagnetic interferences in the X-band was reported by Han et al.[33] MXene has found its importance extensively in the field of energy storage, particularly, as an electrode material for supercapacitors. Yang et al. reported the use of Ti_3C_2/graphene[34] hybrid fibers spun using wet-spinning assembly as an electrode material for supercapacitors, exhibiting a superior volumetric capacitance of 586.4 F cm^{-3}. A flexible supercapacitor electrode was fabricated using surfactant-free $Ti_3C_2T_x$ flakes loaded on a carbonized silk cloth, which exhibited excellent cyclability and flexibility.[35] Thus, MXenes find applications in almost all the areas of science and technology, leaving a space of interest to probe more into the synthesis of MXenes. There are numerous reports in the literature of using carbide-based MXene as supercapacitor electrodes but only few exist for a nitride-based MXene, which may be because of the difficulty in its synthesis.[25,26,36]

In this work, we report a unique and facile protocol to synthesize V_2NT_x MXene and its application as a supercapacitor electrode. The V_2NT_x MXene was obtained by etching Al from its MAX phase V_2AlN. The MAX phase V_2AlN was initially obtained by ball milling vanadium and AlN and further cold pressing them to form a pellet. The pellet was subjected to heat treatment thereafter and this step helps in the densification and reducing the number of structural flaws, such as microvoids and cracks. The pressure applied during cold pressing is found to influence the preferred orientation of the grain during its growth. Al from the MAX phase was etched away to synthesize V_2NT_x MXene. A schematic showing the flowchart of synthesizing V_2NT_x MXene is given in Scheme 1. The as-synthesized V_2NT_x MXene was tested as a supercapacitor electrode using an aqueous electrolyte. A specific capacitance of 112.8 F/g was obtained for the electrode at a

https://dx.doi.org/10.1021/acsomega.0c01215
ACS Omega 2020, 5, 17983−17992

current density of 1.85 mA/cm^2 with an energy density of 15.66 W h/kg and a power density of 3748.4 W/kg.

To further evaluate the potential application of V_2NT_x, an asymmetric supercapacitor (ASC) device was fabricated using V_2NT_x MXene as the negatrode (negative electrode) and Mn_3O_4 nanowalls (NWs) grown on carbon fibers (CFs) as the positrode (positive electrode). With the use of aqueous electrolytes in symmetric supercapacitors, the voltage window is limited as the dissociation of water happens at 1.2 V. This drawback could be overcome with the use of organic electrolytes. Although organic electrolytes help in increasing the potential window, they are not safe to use. ASCs help to overcome this issue by operating at higher voltages in an aqueous electrolyte by combining the potential windows of the two different electrode materials in it. Although the operating voltage of an aqueous symmetric supercapacitor is limited to 1.2 V, an ASC with an aqueous electrolyte can operate beyond 2 V.[37] Generally, carbon is used as the negatrode with a pseudocapacitive material as a positrode in ASCs. The capacitance of the ASC can be increased by replacing the low-capacitive carbon electrode with the MXene electrode.[38] Among the transition metal oxides, manganese oxide, particularly, Mn_3O_4, has gained limelight because of its high specific capacitance, outstanding structural flexibility, abundant nature, low cost, and environmental benignity.[39] Wang et al. reported that Mn_3O_4 nanoparticles synthesized through an ultrasound-assisted method exhibited a specific capacitance of 261 F/g at 0.4 A/g.[40] In the work reported by Qiao et al., porous Mn_3O_4 synthesized via a solvothermal technique exhibited a specific capacitance of 302 F/g at 0.5 A/g with a capacitance retention of 89% even after 5000 cycles.[41] Herein, Mn_3O_4 NWs grown on CF as reported earlier by us[42] were used as the positive electrode with V_2NT_x MXene as the negative electrode in the construction of ASCs. The ASC exhibited a cell voltage of 1.8 V in an aqueous KOH electrolyte.

2. RESULTS AND DISCUSSION

To have a systematic analysis, the ball milling time is varied to study the effect of the same in product formation. The mixture of vanadium and AlN was ball-milled for 8, 15, 20, and 26 h and the X-ray diffraction (XRD) pattern obtained for each of them is shown in Figure 1. XRD for the sample obtained after 26 h of milling has well-defined peaks compared to those obtained for 8, 15, and 20 h, and in this regard, the sample ball-milled for 26 h was chosen for further analysis. In the XRD pattern of the sample ball-milled for 26 h, peaks of vanadium (JCPDS card no: 00-022-1058) and AlN (JCPDS card no: 00-025-1133) could be identified.

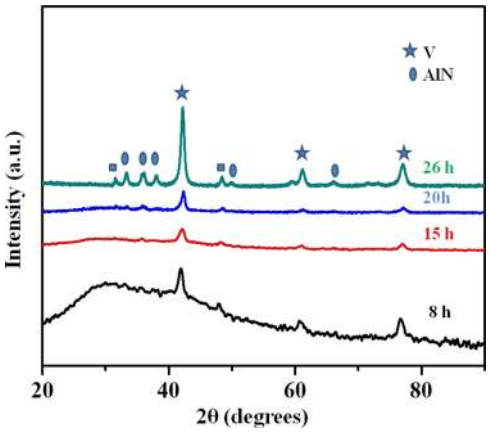

Figure 1. XRD pattern of vanadium and AlN powders ball-milled for different durations of 8, 15, 20, and 26 h.

Figure 2 shows the comparison of XRD obtained for MAX phase V_2AlN, the V_2NT_x obtained after treating with an acid–salt mixture and V_2NT_x obtained after delamination by treating with DMSO. From Figure 2, it can be observed that the XRD pattern obtained for MAX phase V_2AlN is different from that for the carbide MAX phases as there are no peaks (002) in the lower angles. After the MAX phase V_2AlN is subjected to treatment with the LiF–HCl mixture, it can be seen that the number of peaks increased and this can be attributed to the fluoride salt impurities and Al_2O_3 formed during the etching process. Peaks corresponding to Al_2O_3 (JCPDS card no: 00-042-1468) are present in the material, although less intense, because aluminum tends to get easily oxidized leading to the formation of Al_2O_3. The XRD pattern of V_2NT_x MXene subjected to delamination indicates that most of the MAX phase peaks are greatly diminished in intensity and the peaks are slightly shifted to the left.

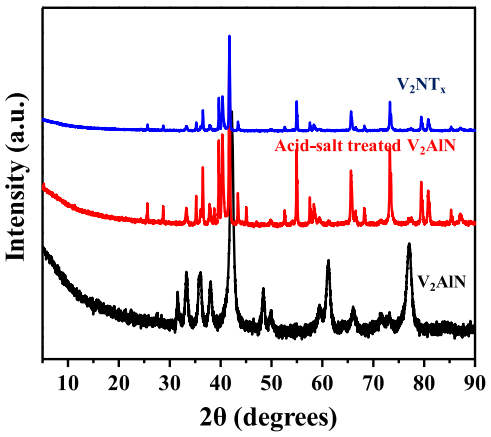

Figure 2. XRD patterns of V_2AlN, acid-salt treated V_2AlN, and V_2NT_x after treating with DMSO.

The morphology of the samples was examined by field emission scanning electron microscopy (FESEM) imaging. The FESEM image of the MAX phase V_2AlN is shown in Figure 3a. Although the layered structure is visible to some extent, they are piled up into blocks of uneven sizes, surface edges, and distribution. The elemental analysis of the sample showed the presence of vanadium, aluminum, and nitrogen in a weight ratio of 2:1:1, respectively (Figure 3b). The elemental mapping in detail is given in Figure S1, which shows the uniform distribution of vanadium, aluminum, and nitrogen. The FESEM image of LiF–HCl-treated V_2AlN is given in Figure 3c. The LiF–HCl solution is capable of etching aluminum from V_2AlN to form a multilayered V_2NT_x MXene. The V_2NT_x MXene here do not possess a perfect lamellar structure as that of carbide MXenes reported but it depicts the formation of 2D layers which are still stacked with uneven edges. The energy-dispersive X-ray spectroscopy (EDAX) spectrum of the acid–salt-treated V_2AlN is shown in Figure 3d. The spectrum shows the presence of surface-terminating groups such as –F and –O as a resultant of acid–salt treatment. The aluminum peak indicates that it is not completely etched after the acid–salt treatment. However,

https://dx.doi.org/10.1021/acsomega.0c01215
ACS Omega 2020, 5, 17983–17992

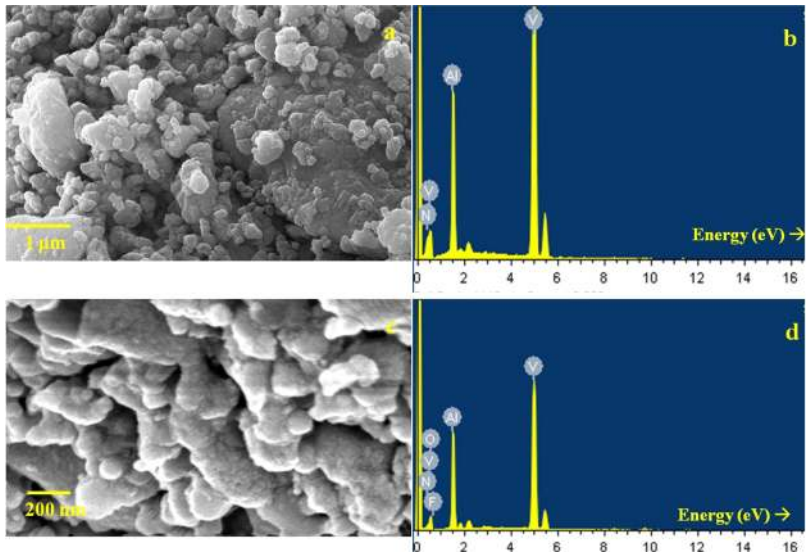

Figure 3. FESEM image (a) and EDAX spectrum (b) of MAX phase V_2AlN; FESEM image (c) and EDAX spectrum (d) of LiF−HCl-treated V_2AlN.

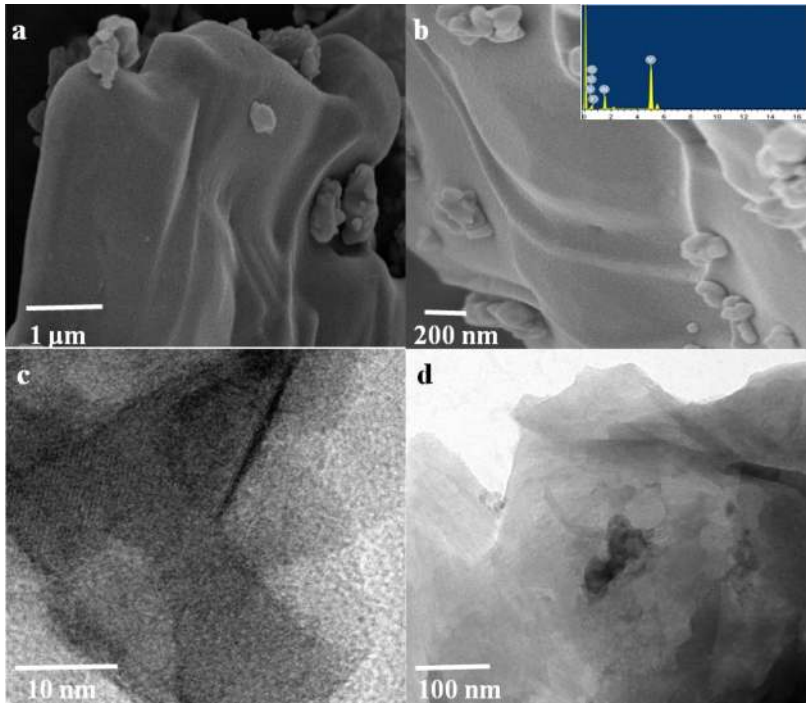

Figure 4. FESEM images (a,b) showing the layered structures of V_2NT_x. Inset (b) shows the EDAX spectrum. (c,d) TEM images of V_2NT_x at different magnifications.

the intensity of the aluminum peak is reduced comparatively. The presence of the carbon peak is due to the use of conductive carbon tape during the analysis. The elemental mapping in detail is given in Figure S2.

Figure 4a−b shows the typical 2D sheet structures obtained after V_2NT_x was treated with DMSO.

Perfect lamellar structures are now visible but with no complete delamination and this could be due to the presence of tiny amounts of Al in the material. The EDAX spectrum of the layered V_2NT_x MXene is given in the inset of Figure 4b. The intensity of the aluminum peak in the EDAX spectrum is further reduced indicating its loss during the exfoliation process. To evaluate the amount of aluminum left on the MXene sheets, inductively coupled plasma−optical emission spectrometry (ICP−OES) analysis was carried out. The percentage amount of aluminum present in the global sample was 9.26%, which was about six times lesser than that of vanadium. This proves the successful formation of V_2N from V_2AlN. The color-coded elemental mapping indicates the uniform distribution of the elements (Figure S3). In order to view the sheets clearly and to further confirm the morphological characteristics, transmission electron microscopy (TEM) analysis was carried out and the images are shown in Figure 4c−d.

The composition and the electronic states of the delaminated V_2NT_x MXene were investigated using X-ray

https://dx.doi.org/10.1021/acsomega.0c01215
ACS Omega 2020, 5, 17983−17992

photoelectron spectroscopy (XPS). CasaXPS software with a shirley background type was used in the XPS peak fitting. The core-level XPS V2p and N1s spectra are depicted in Figure 5.

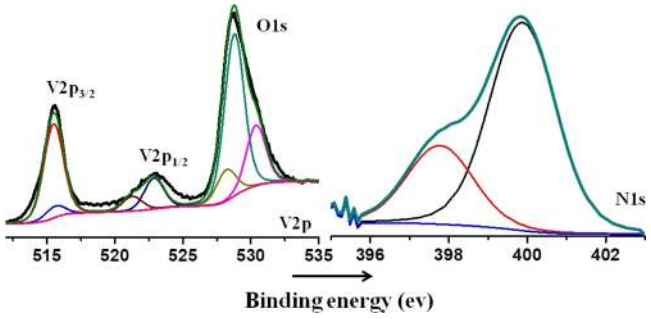

Figure 5. Deconvoluted high-resolution XPS spectra of V2p and N1s.

The V2p regions overlap with the O1s region because of the presence of oxygen on the sample surface and hence they are fitted together. The characteristic peaks at 515.4 and 522.8 eV are ascribed to $V2p_{3/2}$ and $V2p_{1/2}$, respectively. The high intensity peak of O1s at 529 eV indicates the high concentration of oxygen onto the surface of vanadium.[43] With the absence of vanadium oxide peaks in the XRD pattern, it can further be confirmed that functionalization of oxygen has occurred only on the surface and not in the bulk sheets.[44]

The electrochemical performance of V_2NT_x MXene supercapacitor electrodes was examined by slurry-coating V_2NT_x MXene onto CF cloth. The CF cloth is electrically conducting and serves as the current collector for the supercapacitor electrode. The supercapacitive performances of the V_2NT_x MXene electrode are examined using electrochemical impedance spectroscopy (EIS), cyclic voltammetry (CV), and galvanostatic charge−discharge (GCD) measurements. The Nyquist plot of the V_2NT_x MXene electrode is depicted in Figure 6a and the inset shows the Nyquist plot at the magnified high-frequency region. From the Nyquist plot, it can be observed that the V_2NT_x MXene electrode exhibits an electrochemical series resistance (ESR) of 0.4 Ω. The CV curves for the V_2NT_x MXene electrode obtained at different scan rates within a potential window of −1.0 to 0 V are depicted in Figure 6b. The CV curves display nonrectangular profiles with redox peaks which is an evidence of pseudocapacitive charge storage exhibited by the V_2NT_x MXene because of its surface functional groups. The V_2NT_x MXene electrode undergoes faradaic reactions with the

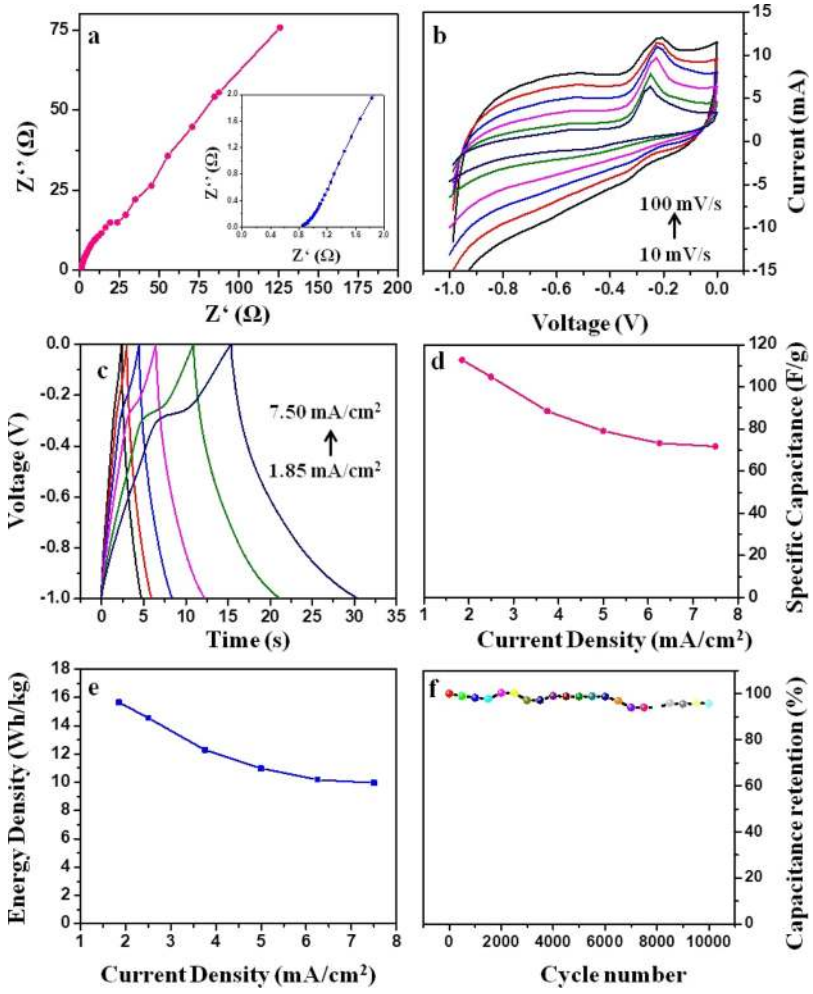

Figure 6. (a) Nyquist plot obtained in a frequency range of 10^6 to 0.02 Hz (inset shows the Nyquist plot in the high-frequency region); (b) CV curves obtained at different scan rates; (c) GCD curves obtained at different current densities of the V_2NT_x MXene electrode; (d) plot of specific capacitance and (e) energy density at different current densities of the V_2NT_x MXene electrode; and (f) plot of capacitance retention at different cycle numbers of the V_2NT_x MXene electrode.

https://dx.doi.org/10.1021/acsomega.0c01215
ACS Omega 2020, 5, 17983−17992

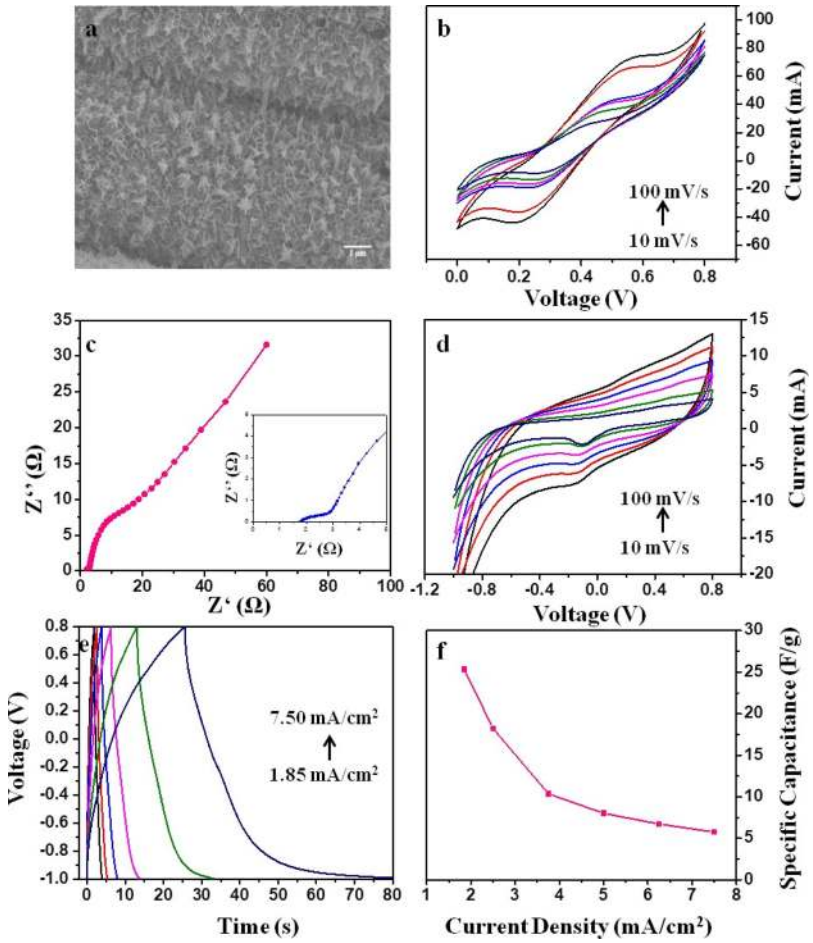

Figure 7. (a) SEM image of Mn_3O_4 NWs grown on CF and (b) CV curves obtained at different scan rates for the Mn_3O_4 NW electrode. (c) Nyquist plot obtained in a frequency range of 10^6 to 0.02 Hz (inset shows the Nyquist plot in the high-frequency region), (d) CV curves obtained at different scan rates, and (e) GCD curves obtained at different current densities of the Mn_3O_4 NWs//V_2NT_x MXene ASC device and (f) plot of specific capacitance obtained at different current densities of the Mn_3O_4 NWs//V_2NT_x MXene ASC device.

electrolyte thereby enhanced charge storage can be obtained. This is due to the presence of functional groups (−F and −O) on the surface of V_2NT_x MXene. Figure 6c shows the GCD curves of the V_2NT_x MXene electrode obtained at different current densities at a potential window of −1.0 to 0 V. The faradaic charge storage possessed by the V_2NT_x MXene electrode is evident from the GCD curves too as it is different from the linear GCD profiles for a typical electrochemical double layer capacitor. The specific capacitance of the V_2NT_x MXene electrode is calculated from these GCD curves and plotted in Figure 6d. A specific capacitance of 112.8 F/g is obtained for the V_2NT_x MXene electrode at a current density of 1.85 mA/cm^2. The capacitance is found to decrease gradually at higher current densities, which is typical for the pseudocapacitors. The energy density at different current densities of the V_2NT_x MXene electrode is plotted in Figure 6e. An energy density of 15.6 W h/kg was obtained at a current density of 1.85 mA/cm^2 with the corresponding power density of 3748.4 W/kg. However, the electrode displayed a high power density of 14,987.4 W/kg at a current density of 7.5 mA/cm^2. In order to examine the electrochemical cycling stability of the electrode, a GCD study was performed for continuous 10,000 cycles at a constant current density of 5 mA/cm^2. The variation in the specific capacitance retention at different cycle numbers is plotted in Figure 6f. A capacitance retention of 96% is observed even after 10,000 cycles, which shows the excellent electrochemical cycling stability of the V_2NT_x MXene electrode. It is well-known that nitride MXenes exhibit remarkable electrochemical stabilities and thus are potential candidates for application in supercapacitors with long cycle life.

An ASC device was fabricated to expand the operating voltage window while using an aqueous electrolyte. It is well-known that a cell voltage >1.2 V cannot be obtained in a symmetric configuration because of the water dissociation. However, the cell voltage can be increased beyond this point by fabricating an ASC device, which utilizes dissimilar electrodes in an aqueous electrolyte. This strategy of fabricating ASCs has advantages of manufacturing supercapacitors with high working voltages in a safe aqueous electrolyte; hence, the flammable organic electrolytes can thus be avoided. We have fabricated an ASC device using V_2NT_x MXene as the negative electrode and Mn_3O_4 NWs grown on CF as the positive electrode and tested in a two-electrode cell configuration using a 3.5 M KOH aqueous electrolyte. The use of Mn_3O_4 NWs grown on CF as an electrode in a symmetric supercapacitor is reported previously.[42] The scanning electron microscopy (SEM) image of Mn_3O_4 NWs grown on CF is shown in Figure 7a from which it can be observed that the Mn_3O_4 NWs are grown on CF uniformly with a porous

https://dx.doi.org/10.1021/acsomega.0c01215
ACS Omega 2020, 5, 17983−17992

architecture. In order to understand the electrochemical performance of the Mn_3O_4 NWs, the CV study is conducted within a potential window of 0−0.8 V in a 3.5 M KOH aqueous electrolyte. The CV curves obtained at different scan rates of the Mn_3O_4 NW electrode are shown in Figure 7b. The curves display typical faradaic charge storage possessed by the Mn_3O_4 NWs with distinguished reduction/oxidation peaks. The faradaic charge storage is helpful in achieving high specific capacitance and energy densities. The supercapacitive performances of the Mn_3O_4 NWs//V_2NT_x MXene ASC device are examined by EIS, CV, and GCD measurements. The Mn_3O_4 NWs//V_2NT_x MXene ASC device was able to operate within a potential window of −1.0 to 0.8 V, thereby obtaining a cell voltage of 1.8 V. The Nyquist plot of the ASC device is depicted in Figure 7c and the inset shows the Nyquist plot in the magnified high-frequency region. From the Nyquist plot, it can be observed that the ASC device exhibits an ESR of 1.5 Ω. The CV curves at different scan rates of the ASC device obtained within a potential window of −1.0 to 0.8 V are depicted in Figure 7d. The CV curves display sloped rectangular profiles with faradaic behavior. Both the electrodes in fabricating the ASC device exhibit pseudocapacitive behavior; hence, the same characteristics can be expected from the ASC device too. Figure 7e shows the GCD curves of the ASC device obtained at different current densities at a potential window of −1.0 to 0.8 V. The nonlinear GCD profiles have also proved the faradaic charge storage possessed by the V_2NT_x MXene and Mn_3O_4 NWs electrodes. The specific capacitance of the Mn_3O_4 NWs//V_2NT_x MXene ASC device is calculated from these GCD curves and plotted in Figure 7f. A specific capacitance of 25.3 F/g is obtained for the ASC device at a current density of 1.85 mA/cm^2. For an ASC device, this value is good as it can work with a cell voltage of 1.8 V. Hence, the V_2NT_x MXene is proven to be a potential candidate for supercapacitor electrodes with long cycle life.

3. CONCLUSIONS

In summary, we have synthesized V_2NT_x MXene by selective etching of Al from V_2AlN by immersing powders of V_2AlN in the LiF−HCl mixture (salt−acid etching) followed by sonication. Delaminated V_2NT_x MXene was obtained by a simple hand-shaking in the DMSO solvent. FESEM images have displayed the layered structure of the V_2NT_x MXene, which was further confirmed through TEM. The V_2NT_x MXene slurry-coated onto CF was used as a supercapacitor electrode. The V_2NT_x MXene electrode displayed a specific capacitance of 112.8 F/g at a current density of 1.85 mA/cm^2 with an energy density of 15.66 W h/kg in a 3.5 M KOH aqueous electrolyte. The electrode exhibited excellent capacitance retention of 96% even after 10,000 charge/discharge cycles. An ASC fabricated with V_2NT_x as the negative electrode and Mn_3O_4 NWs as the positive electrode was able to obtain a cell voltage of 1.8 V in the aqueous KOH electrolyte.

4. EXPERIMENTAL SECTION

4.1. Experimental Reagents. Elemental powders of vanadium (325 mesh, 99.5%) and aluminum nitride (AlN; 10 μm, ≥ 98%), lithium fluoride (LiF, trace metals basis ≥99.99%), isopropyl alcohol (IPA), and DMSO (≥ 99.9%) were purchased from Sigma-Aldrich, India. HCl was purchased from S D Fine-Chem Limited, India. Manganese(II) acetate tetrahydrate (99.99%) *N*-methyl pyrrolidone (NMP, 99.5%) and sodium sulfate (Na_2SO_4, ≥99%) were supplied by Sigma-Aldrich, USA. Super P carbon black and poly(vinylidene fluoride) (PVDF) were supplied by Alfa Aesar, USA.

4.2. Synthesis of V_2AlN. The MAX phase V_2AlN was prepared initially by ball milling the elemental powders of vanadium and AlN at a molar ratio of 2:1 with zirconia balls with a powder-to-ball ratio of 1:20 for 26 h at 250 rpm. The ball-milled precursor was pressed hydraulically to obtain a pellet by applying a pressure of 4 tons. The resultant pellet was maintained at a temperature of 1100 °C for 6 h in a tubular furnace with a ramping rate of 5°/min. The heating was carried out under an argon atmosphere. A solid brick-like pellet was obtained, which was ground thoroughly to form fine powders.

4.3. Synthesis of V_2NT_x. An acid−salt etching of Al with LiF−HCl was carried out as reported previously.[11] In a typical procedure, 0.32 g of LiF was dissolved in 6 M HCl by magnetic stirring for 20 min. To this acid−salt mixture, 0.5 g of the V_2AlN powder was added slowly. This reaction mixture was kept undisturbed for 3 h and during this time, a vigorous reaction between the acid−salt mixture and V_2AlN was observed. Later, the reaction mixture was sonicated for an hour at 40° C and centrifuged several times with water until the supernatant maintained a pH of 6. Finally, the precipitate settled at the bottom of the centrifuge tube was washed with IPA at 4000 rpm and vacuum-filtered to obtain V_2NT_x MXene. The obtained MXene was subjected to delamination by hand-shaking with DMSO for 5 min and then sonicating for 1 h. The solution was then kept undisturbed overnight, centrifuged, and filtered.

4.4. Synthesis of Mn_3O_4 NWs on CF. The electrochemical deposition method was used in the synthesis of two-dimensional Mn_3O_4 NWs on the CF substrate as per the literature.[42] In a typical procedure, an electrochemical deposition bath consisting of 0.16 M Na_2SO_4 and 0.16 M manganese acetate tetrahydrate was used in a three-electrode cell in which a surface-pretreated CF substrate was used as the working electrode, Ag/AgCl was used as the reference electrode, and platinum foil was used as the counter electrode. Mn_3O_4 NWs were deposited at a constant potential of −1.8 V for a period of 20 min through the chronoamperometry technique. The as-synthesized Mn_3O_4 NWs on CF were further washed and dried. Mn_3O_4 NWs grown on CFs were used as the positive electrode for fabricating an ASC in this study.

4.5. Preparation of the V_2NT_x MXene Electrode and Fabrication of V_2NT_x MXene//Mn_3O_4 NW ASC. The V_2NT_x MXene electrode was prepared using the as-synthesized V_2NT_x MXene powder as the electrode-active material. Initially, the V_2NT_x MXene powder, Super P carbon black, and PVDF were taken at a weight ratio of 85, 10, and 5 wt %, respectively, and a slurry was prepared by mixing them together in NMP. The slurry was then coated on to the CF substrate with a geometric area of 2 × 2 cm^2 and dried in an oven thereafter. Here, the CF was used as the current collector. An ASC device was fabricated using V_2NT_x MXene as the negative electrode and Mn_3O_4 NWs as the positive electrode.

4.6. Characterization. XRD analysis was carried out to examine the crystal structure of V_2AlN and V_2NT_x MXene using a Bruker D8 ADVANCE X-ray Diffractometer with Cu Kα radiation. The morphology of the V_2NT_x MXene was examined using a field emission scanning electron microscope imaging (Zeiss) operated at 10 kV equipped with EDAX. The

https://dx.doi.org/10.1021/acsomega.0c01215
ACS Omega 2020, 5, 17983−17992

morphology of the Mn_3O_4 NWs grown on CF was examined using SEM imaging (Zeiss ULTRA-55 FEG SEM). The high-resolution TEM images were captured using an FEI Tecnai, G^2 20 Twin microscope operated at 200 kV. The surface features of the V_2NT_x MXene were studied using XPS (ULVAC-PHI, with an Al Kα (1486.6 eV) X-ray beam spectrometer) and the curve fitting was performed through casaXPS software with the Shirley background type. The electrochemical characterizations of the V_2NT_x MXene electrode, Mn_3O_4 NW electrode, and V_2NT_x MXene//Mn_3O_4 NW ASC device were examined using an electrochemical workstation (SP-150, Bio-Logic Science Instruments).

4.7. Electrochemical Measurement. The electrochemical behavior of the V_2NT_x MXene electrode was examined in a three-electrode cell configuration using a 3.5 M KOH aqueous electrolyte. The V_2NT_x MXene, Ag/AgCl, and Pt foil were used as the working, reference, and counter electrodes, respectively. The EIS analysis of the V_2NT_x MXene electrode was carried out in a frequency range of 10^6 to 0.02 Hz. The CV study of the V_2NT_x MXene electrode was performed within a potential window of −1.0 to 0 V versus Ag/AgCl at different scan rates such as 100, 80, 60, 40, 20, and 10 mV/s. The GCD measurements of the V_2NTx MXene electrode were carried out in a potential window of −1.0 to 0 V at different current densities such as 1.85, 2.50, 3.75, 5.00, 6.25, and 7.50 mA/cm^2. The CV study of the Mn_3O_4/CF electrode was performed within a potential window of 0−0.8 V. The Mn_3O_4 NWs//V_2NT_x MXene ASC device was tested in a two-electrode cell configuration using a 3.5 M KOH aqueous electrolyte. The EIS study of the ASC device was carried out in a frequency range of 10^6 to 0.02 Hz, and the CV study was performed within a potential window of −1.0 to 0.8 V at different scan rates such as 100, 80, 60, 40, 20, and 10 mV/s. The GCD measurement of the ASC device was carried out in a potential window of −1.0−0.8 V at different current densities such as 1.85, 2.50, 3.75, 5.00, 6.25, and 7.50 mA/cm^2. From the GCD curves, the specific capacitance, energy density, and power density were calculated. The specific capacitance was calculated using eq 1.

$$C_{sp} = 2 \times \frac{I \times \Delta t}{\Delta V \times m} \quad (1)$$

where "C_{sp}" is the specific capacitance (in F/g), "I" is the current (in A), "Δt" is the discharging time (in s), "m" is the active mass of the electrode-active material (in g), and "ΔV" is the operating voltage window (in V) of the electrode/ASC device. The energy and power densities were calculated using the following eqs 2 and 3, respectively.

$$E = \frac{1}{2} C_t (\Delta V)^2 \quad (2)$$

$$P = \frac{E}{\Delta t} \quad (3)$$

where "E" is the energy density and P is the power density and all other variables are the same as discussed previously.

■ ASSOCIATED CONTENT

Supporting Information

The Supporting Information is available free of charge at https://pubs.acs.org/doi/10.1021/acsomega.0c01215.

FESEM images and the elemental mapping of V_2AlN; LiF−HCl-treated V_2AlN; and delaminated V_2AlN (PDF)

■ AUTHOR INFORMATION

Corresponding Authors

Soon Kwan Jeong − *Climate Change Technology Research Division, Korea Institute of Energy Research, Daejeon 305-343, South Korea;* orcid.org/0000-0001-5347-3651; Email: jeongsk@kier.re.kr

Andrews Nirmala Grace − *Centre for Nanotechnology Research, Vellore Institute of Technology (VIT), Vellore 632014, Tamil Nadu, India;* orcid.org/0000-0002-2016-3013; Email: anirmalagladys@gmail.com, anirmalagrace@vit.ac.in

Authors

Sandhya Venkateshalu − *Centre for Nanotechnology Research, Vellore Institute of Technology (VIT), Vellore 632014, Tamil Nadu, India*

Jayesh Cherusseri − *NanoScience Technology Center, University of Central Florida, Orlando, Florida 32826, Unites States*

Manickavasakam Karnan − *Functional Materials Division, CSIR-Central Electrochemical Research Institute, Karaikudi 630003, Tamil Nadu, India;* orcid.org/0000-0003-2410-2194

Kowsik Sambath Kumar − *NanoScience Technology Center, University of Central Florida, Orlando, Florida 32826, Unites States*

Pratap Kollu − *School of Physics, University of Hyderabad, Hyderabad 500046, India; Thin Film Magnetism Group, Cavendish Laboratory, Department of Physics, University of Cambridge, Cambridge CB3 0HE, U.K.*

Marappan Sathish − *Functional Materials Division, CSIR-Central Electrochemical Research Institute, Karaikudi 630003, Tamil Nadu, India;* orcid.org/0000-0001-9094-5822

Jayan Thomas − *NanoScience Technology Center, University of Central Florida, Orlando, Florida 32826, Unites States;* orcid.org/0000-0003-3579-6064

Complete contact information is available at: https://pubs.acs.org/10.1021/acsomega.0c01215

Notes

The authors declare no competing financial interest.

■ ACKNOWLEDGMENTS

The authors thank Vellore Institute of Technology (VIT), Vellore, India, for the assistance provided through Research Associate fellowship. S.K.J. acknowledges the research and development program of the Korea Institute of Energy Research (B9-2441) for supporting the work. J.C. acknowledges the P3 Pre-Eminent Postdoctoral Research Fellowship awarded to him by the University of Central Florida.

■ REFERENCES

(1) Dell, R.; Rand, D. A. J. Energy storage — a key technology for global energy sustainability. *J. Power Sources* **2001**, *100*, 2−17.

(2) Stoller, M. D.; Park, S.; Zhu, Y.; An, J.; Ruoff, R. S. Graphene-Based Ultracapacitors. *Nano Lett.* **2008**, *8*, 3498−3502.

(3) Simon, P.; Gogotsi, Y. Materials for electrochemical capacitors. *Nat. Mater.* **2008**, *7*, 845.

(4) Chen, K.; Xue, D. Searching for electrode materials with high electrochemical reactivity. *J. Materiomics* **2015**, *1*, 170−187.

(5) Chaudhari, N. K.; Jin, H.; Kim, B.; San Baek, D.; Joo, S. H.; Lee, K. MXene: an emerging two-dimensional material for future energy conversion and storage applications. *J. Mater. Chem. A* **2017**, *5*, 24564−24579.

(6) Lei, J.-C.; Zhang, X.; Zhou, Z. Recent advances in MXene: Preparation, properties, and applications. *Front. Phys.* **2015**, *10*, 276−286.
(7) Barsoum, M. W. The $M_{N+1}AX_N$ phases: A new class of solids: Thermodynamically stable nanolaminates. *Prog. Solid State Chem.* **2000**, *28*, 201−281.
(8) Naguib, M.; Mochalin, V. N.; Barsoum, M. W.; Gogotsi, Y. 25th Anniversary Article: MXenes: A New Family of Two-Dimensional Materials. *Adv. Mater.* **2014**, *26*, 992−1005.
(9) Hong Ng, V. M.; Huang, H.; Zhou, K.; Lee, P. S.; Que, W.; Xu, J. Z.; Kong, L. B. Recent progress in layered transition metal carbides and/or nitrides (MXenes) and their composites: synthesis and applications. *J. Mater. Chem. A* **2017**, *5*, 3039−3068.
(10) Fredrickson, K. D.; Anasori, B.; Seh, Z. W.; Gogotsi, Y.; Vojvodic, A. Effects of Applied Potential and Water Intercalation on the Surface Chemistry of Ti_2C and Mo_2C MXenes. *J. Phys. Chem. C* **2016**, *120*, 28432−28440.
(11) Ghidiu, M.; Lukatskaya, M. R.; Zhao, M.-Q.; Gogotsi, Y.; Barsoum, M. W. Conductive two-dimensional titanium carbide "clay" with high volumetric capacitance. *Nature* **2014**, *516*, 78.
(12) Urbankowski, P.; Anasori, B.; Makaryan, T.; Er, D.; Kota, S.; Walsh, P. L.; Zhao, M.; Shenoy, V. B.; Barsoum, M. W.; Gogotsi, Y. Synthesis of two-dimensional titanium nitride Ti_4N_3 (MXene). *Nanoscale* **2016**, *8*, 11385−11391.
(13) Soundiraraju, B.; George, B. K. Two-Dimensional Titanium Nitride (Ti_2N) MXene: Synthesis, Characterization, and Potential Application as Surface-Enhanced Raman Scattering Substrate. *ACS Nano* **2017**, *11*, 8892−8900.
(14) Barsoum, M. W.; Radovic, M. Elastic and Mechanical Properties of the MAX Phases. *Annu. Rev. Mater. Res.* **2011**, *41*, 195−227.
(15) Naguib, M.; Mashtalir, O.; Carle, J.; Presser, V.; Lu, J.; Hultman, L.; Gogotsi, Y.; Barsoum, M. W. Two-Dimensional Transition Metal Carbides. *ACS Nano* **2012**, *6*, 1322−1331.
(16) Liu, F.; Zhou, J.; Wang, S.; Wang, B.; Shen, C.; Wang, L.; Hu, Q.; Huang, Q.; Zhou, A. Preparation of High-Purity V_2C MXene and Electrochemical Properties as Li-Ion Batteries. *J. Electrochem. Soc.* **2017**, *164*, A709−A713.
(17) Naguib, M.; Halim, J.; Lu, J.; Cook, K. M.; Hultman, L.; Gogotsi, Y.; Barsoum, M. W. New Two-Dimensional Niobium and Vanadium Carbides as Promising Materials for Li-Ion Batteries. *J. Am. Chem. Soc.* **2013**, *135*, 15966−15969.
(18) Seh, Z. W.; Fredrickson, K. D.; Anasori, B.; Kibsgaard, J.; Strickler, A. L.; Lukatskaya, M. R.; Gogotsi, Y.; Jaramillo, T. F.; Vojvodic, A. Two-Dimensional Molybdenum Carbide (MXene) as an Efficient Electrocatalyst for Hydrogen Evolution. *ACS Energy Lett.* **2016**, *1*, 589−594.
(19) Zhou, J.; Zha, X.; Chen, F. Y.; Ye, Q.; Eklund, P.; Du, S.; Huang, Q. A Two-Dimensional Zirconium Carbide by Selective Etching of Al_3C_3 from Nanolaminated $Zr_3Al_3C_5$. *Angew. Chem., Int. Ed.* **2016**, *55*, 5008−5013.
(20) Yang, J.; Naguib, M.; Ghidiu, M.; Pan, L.-M.; Gu, J.; Nanda, J.; Halim, J.; Gogotsi, Y.; Barsoum, M. W. Two-Dimensional Nb-Based M_4C_3 Solid Solutions (MXenes). *J. Am. Ceram. Soc.* **2016**, *99*, 660−666.
(21) Zhou, J.; Zha, X.; Zhou, X.; Chen, F.; Gao, G.; Wang, S.; Shen, C.; Chen, T.; Zhi, C.; Eklund, P.; Du, S.; Xue, J.; Shi, W.; Chai, Z.; Huang, Q. Synthesis and Electrochemical Properties of Two-Dimensional Hafnium Carbide. *ACS Nano* **2017**, *11*, 3841−3850.
(22) Anasori, B.; Xie, Y.; Beidaghi, M.; Lu, J.; Hosler, B. C.; Hultman, L.; Kent, P. R. C.; Gogotsi, Y.; Barsoum, M. W. Two-Dimensional, Ordered, Double Transition Metals Carbides (MXenes). *ACS Nano* **2015**, *9*, 9507−9516.
(23) Meshkian, R.; Tao, Q.; Dahlqvist, M.; Lu, J.; Hultman, L.; Rosen, J. Theoretical stability and materials synthesis of a chemically ordered MAX phase, Mo_2ScAlC_2, and its two-dimensional derivate Mo_2ScC_2 MXene. *Acta Mater.* **2017**, *125*, 476−480.
(24) Naguib, M.; Unocic, R. R.; Armstrong, B. L.; Nanda, J. Large-scale delamination of multi-layers transition metal carbides and carbonitrides "MXenes". *Dalton Trans.* **2015**, *44*, 9353−9358.
(25) Djire, A.; Zhang, H.; Liu, J.; Miller, E. M.; Neale, N. R. Electrocatalytic and Optoelectronic Characteristics of the Two-Dimensional Titanium Nitride $Ti_4N_3T_x$ MXene. *ACS Appl. Mater. Interfaces* **2019**, *11*, 11812−11823.
(26) Djire, A.; Bos, A.; Liu, J.; Zhang, H.; Miller, E. M.; Neale, N. R. Pseudocapacitive Storage in Nanolayered Ti_2NT_x MXene Using Mg-Ion Electrolyte. *ACS Appl. Nano Mater.* **2019**, *2*, 2785−2795.
(27) Urbankowski, P.; Anasori, B.; Hantanasirisakul, K.; Yang, L.; Zhang, L.; Haines, B.; May, S. J.; Billinge, S. J. L.; Gogotsi, Y. 2D molybdenum and vanadium nitrides synthesized by ammoniation of 2D transition metal carbides (MXenes). *Nanoscale* **2017**, *9*, 17722−17730.
(28) (a) Mashtalir, O.; Naguib, M.; Mochalin, V. N.; Dall'Agnese, Y.; Heon, M.; Barsoum, M. W.; Gogotsi, Y. Intercalation and delamination of layered carbides and carbonitrides. *Nat. Commun.* **2013**, *4*, 1716. (b) Wang, X.; Kajiyama, S.; Iinuma, H.; Hosono, E.; Oro, S.; Moriguchi, I.; Okubo, M.; Yamada, A. Pseudocapacitance of MXene nanosheets for high-power sodium-ion hybrid capacitors. *Nat. Commun.* **2015**, *6*, 6544. (c) Lukatskaya, M. R.; Dunn, B.; Gogotsi, Y. Multidimensional materials and device architectures for future hybrid energy storage. *Nat. Commun.* **2016**, *7*, 12647.
(29) Xie, Y.; Dall'Agnese, Y.; Naguib, M.; Gogotsi, Y.; Barsoum, M. W.; Zhuang, H. L.; Kent, P. R. C. Prediction and Characterization of MXene Nanosheet Anodes for Non-Lithium-Ion Batteries. *ACS Nano* **2014**, *8*, 9606−9615.
(30) Guo, Z.; Zhou, J.; Zhu, L.; Sun, Z. MXene: a promising photocatalyst for water splitting. *J. Mater. Chem. A* **2016**, *4*, 11446−11452.
(31) Rasool, K.; Helal, M.; Ali, A.; Ren, C. E.; Gogotsi, Y.; Mahmoud, K. A. Antibacterial Activity of $Ti_3C_2T_x$ MXene. *ACS Nano* **2016**, *10*, 3674−3684.
(32) Xu, B.; Zhu, M.; Zhang, W.; Zhen, X.; Pei, Z.; Xue, Q.; Zhi, C.; Shi, P. Ultrathin MXene-Micropattern-Based Field-Effect Transistor for Probing Neural Activity. *Adv. Mater.* **2016**, *28*, 3333−3339.
(33) Han, M.; Yin, X.; Wu, H.; Hou, Z.; Song, C.; Li, X.; Zhang, L.; Cheng, L. Ti_3C_2 MXenes with Modified Surface for High-Performance Electromagnetic Absorption and Shielding in the X-Band. *ACS Appl. Mater. Interfaces* **2016**, *8*, 21011−21019.
(34) Yang, Q.; Xu, Z.; Fang, B.; Huang, T.; Cai, S.; Chen, H.; Liu, Y.; Gopalsamy, K.; Gao, W.; Gao, C. MXene/graphene hybrid fibers for high performance flexible supercapacitors. *J. Mater. Chem. A* **2017**, *5*, 22113−22119.
(35) Hu, M.; Hu, T.; Cheng, R.; Yang, J.; Cui, C.; Zhang, C.; Wang, X. MXene-coated silk-derived carbon cloth toward flexible electrode for supercapacitor application. *J. Energy Chem.* **2018**, *27*, 161−166.
(36) (a) Li, L.; Zhang, N.; Zhang, M.; Wu, L.; Zhang, X.; Zhang, Z. Ag-Nanoparticle-Decorated 2D Titanium Carbide (MXene) with Superior Electrochemical Performance for Supercapacitors. *ACS Sustainable Chem. Eng.* **2018**, *6*, 7442−7450. (b) Wang, Y.; Dou, H.; Wang, J.; Ding, B.; Xu, Y.; Chang, Z.; Hao, X. Three-dimensional porous MXene/layered double hydroxide composite for high performance supercapacitors. *J. Power Sources* **2016**, *327*, 221−228.
(37) Wang, F.; Xiao, S.; Hou, Y.; Hu, C.; Liu, L.; Wu, Y. Electrode materials for aqueous asymmetric supercapacitors. *RSC Adv* **2013**, *3*, 13059.
(38) Lukatskaya, M. R.; Kota, S.; Lin, Z.; Zhao, M.-Q.; Shpigel, N.; Levi, M. D.; Halim, J.; Taberna, P.-L.; Barsoum, M. W.; Simon, P.; Gogotsi, Y. Ultra-high-rate pseudocapacitive energy storage in two-dimensional transition metal carbides. *Nat. Energy* **2017**, *2*, 17105.
(39) Dessie, Y.; Tadesse, S.; Eswaramoorthy, R. Review on manganese oxide based biocatalyst in microbial fuel cell: Nanocomposite approach. *Mater. Sci. Energy Technol.* **2020**, *3*, 136−149.
(40) Wang, L.; Chen, L.; Li, Y.; Ji, H.; Yang, G. Preparation of Mn_3O_4 nanoparticles at room condition for supercapacitor application. *Powder Technol.* **2013**, *235*, 76−81.

https://dx.doi.org/10.1021/acsomega.0c01215
ACS Omega 2020, 5, 17983−17992

(41) Qiao, Y.; Sun, Q.; Xi, J.; Cui, H.; Tang, Y.; Wang, X. A modified solvothermal synthesis of porous Mn_3O_4 for supercapacitor with excellent rate capability and long cycle life. *J. Alloys Compd.* **2016**, *660*, 416.
(42) Sambath Kumar, K.; Cherusseri, J.; Thomas, J. Two-Dimensional Mn_3O_4 Nanowalls Grown on Carbon Fibers as Electrodes for Flexible Supercapacitors. *ACS Omega* **2019**, *4*, 4472−4480.
(43) Kumar, R. A.; Babu, K. S.; Dasgupta, A.; Ramaseshan, R. Enhancing the dual magnetic and optical properties of co-doped cerium oxide nanostructures. *RSC Adv.* **2015**, *5*, 103465−103473.
(44) Mahesh, K. V.; Rashada, R.; Kiran, M.; Peer Mohamed, A.; Ananthakumar, S. Shear induced micromechanical synthesis of Ti_3SiC_2 MAXene nanosheets for functional applications. *RSC Adv.* **2015**, *5*, 51242−51247.

https://dx.doi.org/10.1021/acsomega.0c01215
ACS Omega 2020, 5, 17983−17992